Compact Vector Magnetometer for Pico Satellites

Klaus Krogsgaard

Measurement & Instrumentation, Ørsted•DTU

Technical University of Denmark (DTU)

Advisors – Associated Professors José M. G. Merayo & Peter Brauer

Abstract: *A small vector magnetometer has been constructed for DTUsat – a Danish CubeSat student project at the Technical University of Denmark. The presented magnetometer is used for attitude determination in conjunction with sun sensors, and supply local field measurements for the magnetotorquer controller. Present launch date is June 30th, 2003 from Plesetsk, Russia.*

Constraints on mechanical size, mass, and power consumption due to the small satellite outline have lead to the development of a highly integrated magnetometer system. Excellent performance is achieved using integrated magnetoresistive thin film sensors with on-chip bias coil. Accuracy better than 50nT over the full operating range of -10° C to 70° C is achieved through careful circuit design and compensation in both hardware and software. The single PCB holds all magnetometer circuits including sensors, measurement circuits, synchronous serial interface for control and readout, and latch-up detection.

This paper describes design, circuit topology, performance tests, and satellite level calibration of the vector magnetometer.

1 Introduction

The trend of today's satellites for educational and scientific purposes is ever smaller satellites – without compromising performance or functionality. This development is driven by the constant miniaturization of electronics and the financial benefits of small satellites: launch costs are low and projects can easily be fitted in as secondary, tertiary or lower payloads on future launches.

Most satellite missions require some form of attitude control due to the communication system and/ or payloads. The geomagnetic field strength can for LEO satellites be used for attitude determination and momentum unloading through magnetotorquers/torqrods. Both require means of determining the local magnetic field strength vector, and in many cases the simplest approach is to use an on-board magnetometer.

High precision attitude determination with e.g. GPS and star imagers is not feasible for small satellites due to mass, size and/or power consumption; same goes for magnetometers designed for high precision measurements as e.g. Ørsted's CSC flux-gate magnetometer. When utilizing a magnetometer for attitude determination, the required accuracy is in the order of $50 - 500nT$ which corresponds to $0.2 - 2°$. Using magnetometers in conjunction with magnetotorquers/torqrods solely for momentum unloading requires only moderate accuracy. This is due to the closed loop operation of the complete ACDS which attenuates actuator noise introduced by the limited accuracy.

The magnetometer presented in this paper and shown in figure 1 takes advantage of thin film sensors developed over the last decade, which are currently commercially available in highly integrated solutions. These small sensors are utilized to achieve a very compact magnetometer, and the selected sensor chip enables the use of different compensation principles to greatly improve performance.
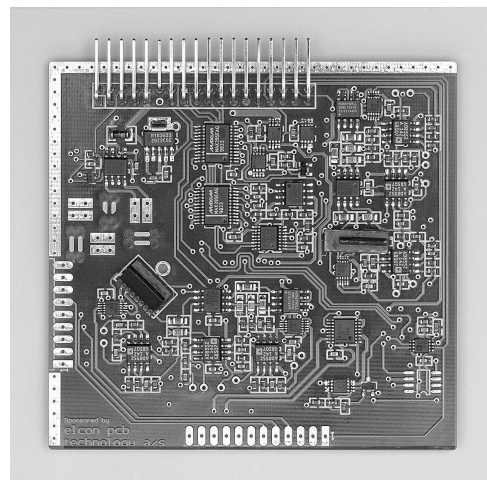

Figure 1: DTUsat ACDS main board.

2 The DTUsat Project

A number of students and supervisors formed in the summer of 2001 a project group in an attempt to design and produce the first satellite project

made and organized mainly by students at the Technical University of Denmark (DTU) – hence the name DTUsat.

Very early in the project it was decided to use the CubeSat concept which gives all the basic mechanical constraints. This concept ensures standardization and flexibility enabling launch companies to reduce launch cost of the individual satellite to 35000-70000$, making it feasible for small organizations and universities to start their own satellite projects.

The DTUsat project has now entered the final phase; after two years work, the satellite is build and shipped to Plesetsk, Russia where it is to be launched on June 30th, 2003. The expected dusk-dawn orbit has an altitude of approximately 900km and enables radio contact with the ground segment in Denmark 2-6 times per day, each with a duration of around 10 minutes.

Throughout the project students have been organized in small groups, each working on a specific subsystem as parts of special courses under guidance by one or more supervisors. Each group operates and organizes the work independently of other groups, with the system engineering group as the common forum, where representatives from all groups meet once a week. Global system issues and coordination between groups are handled at these meetings to ensure compatibility and internal design reviews.

On-board hardware has been divided into five subsystems, each on its own PCB:

Power utilizes solar cells mounted on four sides capable of delivering approximately 1.5W. Besides driving the satellite via a DC-DC converter, these also charge the on-board Li-Ion battery. The battery provides additional capacity during radio transmissions, where power consumption exceeds the available solar energy. Latch-up protection is integrated into the power subsystem and shuts down the entire satellite in case of a latch-up.

On-Board Computer consists of a conventional microprocessor system with processor, boot-ROM, RAM, and Flash-RAM. This PCB also serves as a back plane, where supply connections etc. are routed through. The control of other subsystems is mainly carried out through a shared synchronous serial bus, and a 1-wire bus for temperature sensors.

Radio uses a traditional single-band transceiver layout. In agreement with AMSAT, communications with the ground segment is done at 437.475MHz using 2400bps simplex. The circular polarized antenna mounted on one side of the satellite is sufficiently omnidirectional to operate without attitude control.

Attitude contains three main parts: magnetometer, sun sensors, and magnetotorquers with driver. Magnetometer, sun sensor interface and magnetotorquer driver are all integrated on the main PCB. Each of the five two-axis angular sun sensors are mounted on small PCBs containing amplifiers and A/D converters connected to the interface of the main PCB. The PWM driven magnetotorquers are mounted on the inside of three side panels and are capable of approximately 1μNm of control torq.

Tether Payload is the scientific mission of the satellite. 1-2 months after launch, this 500m long electrodynamic tether will be deployed, enabling the lowering of the satellite altitude at a rate of a few kilometers per week.

2.1 Attitude Subsystem

The complete ACDS system consists of both hardware and software as shown in figure 2.

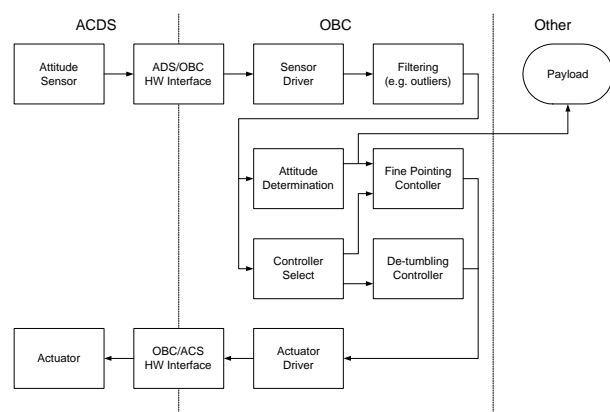

Figure 2: Block diagram of the DTUsat ACDS.

This topology eliminates the need for a dedicated ACDS processor by using the main processor. Benefits are a reduction in hardware complexity and power consumption, and it eliminates the need for two software platforms. However, it requires sufficient processing power to ensure real-time calculations of attitude determination and control.

The mechanical and electrical constraints of the ACDS main board is listed below:

- Maximum mass: 35g

- PCB size: 80mm by 84mm

- Component height: 5.5mm/2.5mm

- Average power consumption: 70mW

3 Requirements

Two main requirements for the magnetometer is indirectly given by the DTUsat project: range and accuracy. Being in LEO, the effective dynamic range must be ±50000nT or more. The needed attitude determination accuracy of 1° sets the other value; using a simple two-dimensional approximation and minimum geomagnetic field, this accuracy translates to 300nT on all axes.

After initial testing of sensor and prototype circuit, the design goals were increased to a range of no less than ±64000nT and accuracy of approximately 50nT.

4 Magnetoresistive Sensor

Selecting the correct sensor type is essential for the achievable performance of the magnetometer. Both Hall sensors and flux gates were considered, but the choice fell on the magnetoresistive sensor type due to constraints and requirements. This sensor offers small size with moderate accuracy and field range, which is just right for this application.

Magnetoresistive sensors are generally highly integrated thin film components using Permalloy (80% Ni, 20% Fe). Permalloy is a high permeability material ($\mu_r \approx 80000$) and is often used as core material for integrated inductors. Magnetoresistive sensors utilizes that Permalloy resistivity changes with field strength in the sensitive direction, which is defined during deposition by aligning all magnetic domains within the thin film. As with many other resistive sensors, most magnetoresistive sensors consists of four magnetoresistive elements in Wheatstone bridge configuration to reduce temperature dependency. The range of the sensors is limited ($\approx$ 1mT) since large fields are able to change the alignment of the magnetic domains. Sensitivity of the sensors is however fairly high ($\approx$ 20nT) but so is the noise, largely due to thermal noise of the resistive sensor. Typical applications includes navigation systems as electronical compasses.

Integrated magnetoresistive sensors are manufactured by e.g. Philips and Honeywell. Based on datasheet specifications, the HMC1021 sensor from Honeywell was selected – largely due to its ability to operate at low supply voltage ($\geq$ 3.3V) and integrated coils for both re-alignment of magnetic domains and bias field. Another useful feature of the HMC1021 sensor is the different package versions: HMC1021S is an ordinary surface mounted SO-8 package version, while HMC1021Z is a fine-pitch SIP-8 package version. This allows for easy mounting of all three orthogonal sensor axis.

Initial verification of the sensors were done using an early prototype, to verify datasheet specifications. Radiation hardness with respect to total dose was also tested to ensure minimal drift during the operation time of the magnetometer; no changes were detected at doses up to 10krad.

With the chosen sensor type, two potential error sources arise:

- Sensor offset due to bridge imbalance, or rather the temperature drift of any offset that might exist as this cannot be removed by simple calibration.

- Linearity error over the required range and any temperature dependency of this. Compensating this by calibration would require a large number of coefficients and/or computations.

The following describes how the needed compensations can be achieved by utilizing the features of the sensor material and sensor chip.

4.1 Offset Compensation

According to the datasheet typical sensor offset are ±50000nT. This implies the need for expanding the measuring range beyond ±100000nT and thus require an A/D converter with higher effective resolution. The best way to minimize this offset is to introduce a hardware compensation in the form of balancing resistors connected parallel to the sensor bridge.

However, additional compensation is needed since this does not remove the temperature drift. This is achieved by making full use of the Permalloy material: by re-applying a strong magnetic field perpendicular to the direction of sensitivity, the alignment of the magnetic domains within the thin film can be completely reversed without influencing the absolute sensitivity. The result is a sensitivity with opposite sign. This feature can be used by first making a measurement in one state (e.g. the Reset state), reversing the alignment and making a second measurement (the Set state). The actual field strength can then be calculated as the difference between the two measurements divided by two. Since the offset remains constant it is canceled out by taking the difference between the two measurements.

The magnetic field for re-aligning the magnetic domains must exceed 1mT. A coil specifically designed for this is integrated on the sensor chip; the reversal can be achieved by applying a 0.5A current pulse to the coil for $2 - 10\mu s$. Additionally, each re-alignment ensures optimal alignment in the direction of sensitivity, thus gaining maximum sensor sensitivity.

4.2 Linearity Compensation

The intrinsic field-to-resistance characteristic of Permalloy is highly non-linear – it actually exhibit a second degree polynomial characteristic at low field strengths with maximum resistance at 0T. Secondly, this means that only the absolute field strength in the sensitive direction can be measured. In order to obtain a fairly linear characteristic and enabling detection of field direction, a pattern of conducting strips is placed on top of the Permalloy film.

The remaining non-linearities are – compared to the offset error – fairly small, but cannot be completely disregarded. The HMC1021 datasheet states a typical linearity error of 100nT over a range of ±100000nT, which is within the requirements of 300nT for the magnetometer. The margin for component variations is however small, making compensation necessary. The compensation principle employed is similar to that of the flux gate: A known bias field is controlled using the sensor signal as feedback. The bias field cancels the external field, making the sensor operate in a 0T field at all times if no additional offset errors are present. In the event of offset, the constant field strength of operation is determined by the amount of error.

The bias field can easily be generated by using the second coil integrated on the sensor chip. This coil is closely coupled to the sensor making it possible to generate a fairly large bias field with a small current: 5mA coil current generates a bias field of approximately 100000nT.

The magnitude of the bias coil current is relative simple to measure. Due to the linear relation between coil current and generated field strength, the measured value is directly related to the canceling bias field strength and thus the external field strength. The required range of the measuring circuit is approximately ±3.2mA plus additional range for offset errors, and an accuracy of at least 15μA.

5 Circuit Topology

The magnetometer has three main axes and one extra for redundancy. Ideally, main axes form an orthogonal frame while the redundancy axis is mounted at an angle. This enables the redundancy axis to replace any main axis with only minor loss of accuracy. The topology for all axes is shown in figure 3.
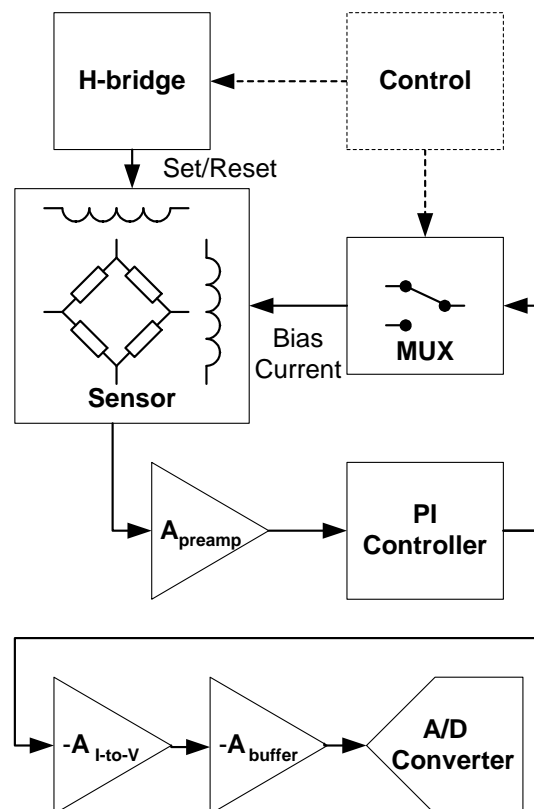

Figure 3: Block diagram of the magnetometer HW.

The PI control loop and analog multiplexer are the key parts in the implementation of the compensation principles.

Practical implementation of the linearity compensation principle described earlier is done directly in hardware by utilizing a PI controller. This controller type has no inherent steady state error and is very simple to implement using modern operational amplifiers. The selected amplifier is capable of delivering the needed coil current and does not need additional buffering.

The offset compensation described earlier involves changing the sign of the sensor sensitivity, effectively changing the negative feedback of the PI control loop to positive feedback. A low ohmic, analog multiplexer is placed in series with both terminals of the bias coil; placing the multiplexer

here also reduces the influence of any leakage currents. By switching the terminals in accordance with the sensor sensitivity sign, negative feedback for both sensor states is maintained.

Implementation of both compensation principles changes the offset compensation principle described earlier: actual field strength must be calculated as the sum of the two coil current divided by two. The drawback of this slight alteration is, that any offset error introduced after the PI control loop no longer is removed in the final calculation. However, phase reversal of the signal from the PI controller is achieved by connecting the multiplexer properly and thereby regaining the offset compensation of the last three blocks in the signal path.

The magnetometer makes one full vector measurement per second, after which it is powered down to reduce power consumption. A compromise between fast settling time leading to low power consumption, and high frequency noise attenuation has been achieved by using a combination of hardware and software filtering; the resulting measurement time is approximately 20ms.

6 Compensation Principles

The system equations for the magnetometer measurement circuit are given below and form the basis for the offset compensation principle; operating the sensor in constant field to compensate for linearity is directly achieved by using the PI controller. Variables A_i are gain factors for amplifier stages, and S_i are sensitivities of the sensor; $\pm$ or $\mp$ indicates change in sign depending on sensor state, with the upper sign being in the reset state.

Deriving the PI controller's point of operation and the A/D converter output in engineering units:

$$
\begin{aligned}
B_{tot} &= -B_{ext} + B_{bias} \\
V_{sensor} &= \pm S_{sensor} B_{tot} + V_{offset,sensor} \\
V_{preamp} &= A_{preamp}(V_{sensor} + V_{offset,preamp}) \\
V_{PI,error} &= -V_{preamp} + V_{offset,PI} \\
B_{bias} &= \pm S_{bias} I_{bias} \\
\Rightarrow V_{PI,error} &= \mp A_{preamp} S_{sensor}(-B_{ext} \pm S_{bias} I_{bias}) \\
&\quad + V_{offset,loop} \\
\Rightarrow I_{bias} &= \pm \frac{B_{ext}}{S_{bias}} + \frac{V_{offset,loop}}{A_{preamp} S_{sensor} S_{bias}}
\end{aligned}
\tag{1}
$$

$$
\begin{aligned}
V_{I-to-V} &= -A_{I-to-V} I_{bias} + V_{offset,I-to-V} \\
V_{buffer} &= -A_{buffer}(V_{I-to-V} + V_{offset,buffer}) \\
EU_{ADC} &= \frac{V_{buffer} + V_{offset,ADC}}{V_{LSB}} \\
\Rightarrow EU_{ADC} &= \pm \frac{A_{buffer} A_{I-to-V}}{S_{bias} V_{LSB}} B_{ext} + \frac{V_{offset}}{V_{LSB}}
\end{aligned}
\tag{2}
$$

The variable V_{offset} incorporates all offset errors of the system and can be expanded as shown below:

$$
\begin{aligned}
V_{offset} = &-\frac{A_{buffer} A_{I-to-V}}{S_{sensor} S_{bias}} V_{offset,sensor} \\
&-\frac{A_{buffer} A_{I-to-V}}{S_{sensor} S_{bias}} V_{offset,preamp} \\
&+\frac{A_{buffer} A_{I-to-V}}{A_{preamp} S_{sensor} S_{bias}} V_{offset,PI} \\
&- A_{buffer} V_{offset,I-to-V} \\
&- A_{buffer} V_{offset,buffer} \\
&+ V_{offset,ADC}
\end{aligned}
\tag{3}
$$

Variables A_i, S_i, $V_{offset,i}$, and V_{LSB} should in theory remain almost constant, showing only temperature dependencies, making the second term in equation (2) a "simple" function of temperature.

6.1 Offset Compensation

Assuming constant temperature enables relative simple compensation of the offset error in equation (2) by calculating the difference between reset and set state measurements:

$$
\begin{aligned}
EU_{comp} &= \frac{EU_{ADC,reset} - EU_{ADC,set}}{2} \\
&= \frac{1}{2}\left(\left(\frac{A_{buffer} A_{I-to-V}}{S_{bias} V_{LSB}} B_{ext} + \frac{V_{offset}}{V_{LSB}} \right) \right. \\
&\quad \left. - \left(-\frac{A_{buffer} A_{I-to-V}}{S_{bias} V_{LSB}} B_{ext} + \frac{V_{offset}}{V_{LSB}} \right) \right) \\
&= \frac{A_{buffer} A_{I-to-V}}{S_{bias} V_{LSB}} B_{ext}
\end{aligned}
\tag{4}
$$

Measurements for both sensor states are acquired sequentially, ensuring time delays in the order of 10ms between measurement pairs. This delay is very small compared to the thermal time constant of the satellite, making the assumption of constant temperature for a single measurement pair a good approximation.

6.2 Scale Factor Drift

The scaling factor $\frac{A_{buffer} A_{I-to-V}}{S_{bias} V_{LSB}}$ in equations (2) and (4) remains temperature dependent. Characterising this is complex and not possible for the DTUsat project, but the temperature dependencies are minimized by careful circuit design:

- V_{LSB} is defined by the 1.25V voltage reference; temperature coefficient of this is according to datasheet below 5ppm

- V_{LSB} is common to all four axes and will as such scale linearly and only change the magnitude of the measured field vector, leaving the direction unchanged

- A_{buffer} and A_{I-to-V} are the same for all four axes and implemented using resistors from the same batches; the assumption is, that temperature coefficient remains fairly constant for a single batch. This leads to linear scaling of all axes, again changing only magnitude and not direction of the field vector.

- S_{bias} defines the sensitivity of the bias/offset coil and is linked to the individual sensor. The field generated is by definition given by mechanical dimensions of the coil and distance to sensor elements. As both sensor elements and coil is implemented on the same chip die, distance changes with the thermal expansion of silicon which is approximately 3ppm/K.

7 Performance

Laboratory tests are all done using a magnetic shield made from high permeability metal. Where needed, temperature control is achieved by using a non-magnetic cooler/heated chamber containing the magnetometer within the shield. The chamber is insulated to minimize both temperature gradients within the chamber and temperature changes of the magnetic shield; the latter would lead to changes in the magnetic residual of the shield, and thereby add yet another variable.

7.1 Electrical Offset

The electrical offset does not result in measurement error as it is removed by the compensation. However, it remains a part of the measured values in both reset and set state, reducing the effective dynamic range which still must meet the design goal of ±64000nT.

Selecting sensors from a larger batch resulted in initial offset of less than 14000nT at room temperature. Thanks to this selection, total electrical offset can be kept below 16000nT over the full temperature range as shown in figure 4. This corresponds to a reduction in dynamic range of 20% when neglecting magnetic offset.

Electrical offset is highly temperature dependent. Worst-case linearity error is approximately
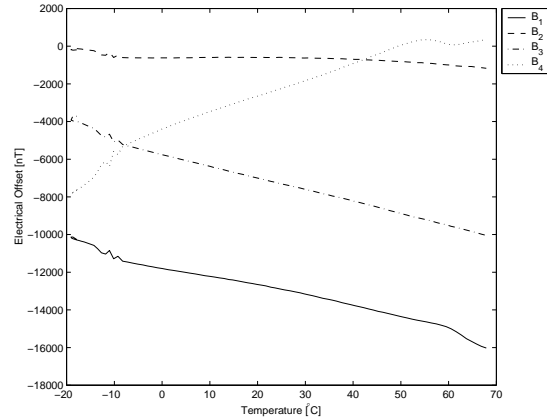

Figure 4: Electrical offset.

1200nT making it unsuitable for precision measurements, but in case of in-flight malfunction of the set/reset circuit, linearity error does remain sufficiently low to make it a usable backup option if the implemented redundant fourth axis also malfunctions.

7.2 Magnetic Offset

After compensation of electrical offset, only magnetic offset remains which can be caused by a number of things:

- Uncertainties associated with the re-alignment of the magnetic domains of the sensor elements during state changes. This can be improved by using a larger set/reset current pulse, which unfortunately is impossible with the given constraints.

- Small current loops in the ACDS main board subsystems generate additional offset fields in close proximity to the sensors.

- When integrated into the satellite, magnetic offset is also generated by ferromagnetic elements e.g. the Li-Ion battery and current loops of other subsystems.

The measured magnetic offset is shown in figure 5. Absolute offset is below 800nT over the full temperature range, which is significantly less than the electrical offset. More importantly, temperature dependency for magnetic offset is highly linear with linearity error below approximately 30nT as shown in figure 6. This enables an almost complete removal of magnetic offset by using a simple linear model implemented in the data processing of the measurements, when converting these into magnetic field vectors. See section 7.4 for details concerning the large deviation at low temperature.
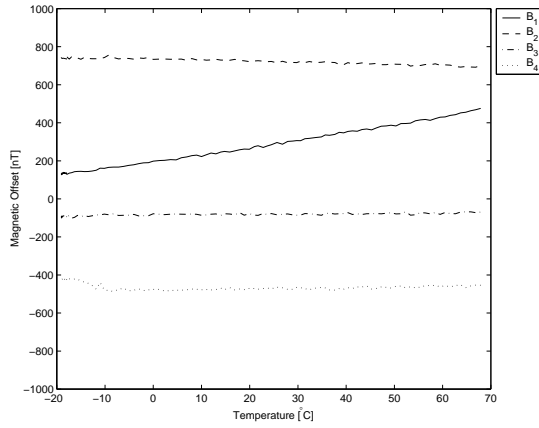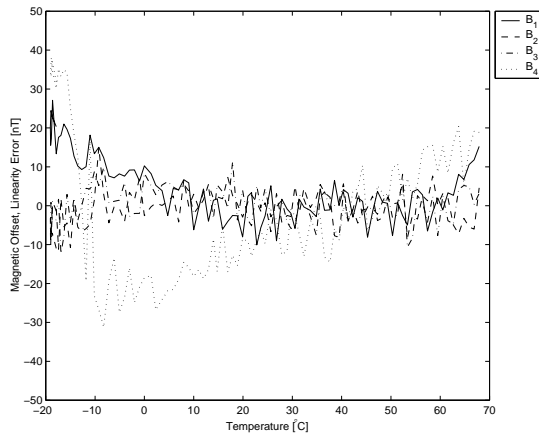
Figure 5: Magnetic offset.
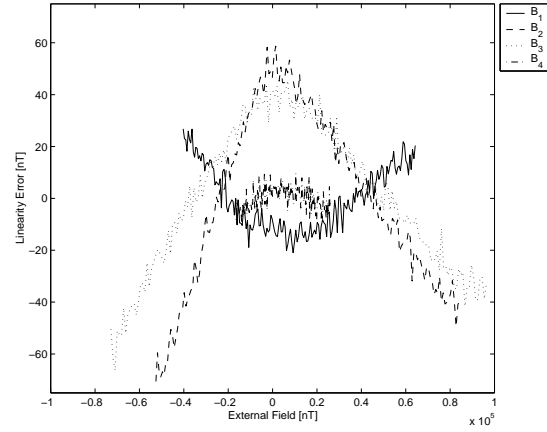

Figure 6: Linearity error for magnetic offset.

Figure 7: Linearity error.

part of the temperature range: $12 - 15\text{nT}_{RMS}$ or approximately 45nT_{peak}.
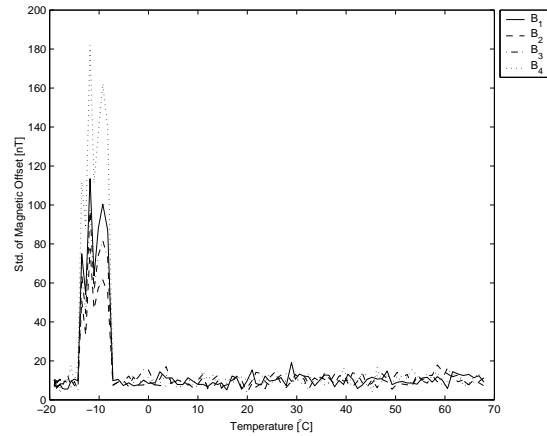
Figure 8: Standard deviation for magnetic offset.

7.3 Linearity

Linearity tests are done using a simple three-axis coil system, which can be placed within the magnetic shield. This is unfortunately not without worries as e.g. saturation of the shield can result in large errors. Further studies are required to verify the validity of this test procedure.

The measured linearity errors for all four axes is shown in figure 7. This shows errors of up to 60nT over the full field range, but the very linear slopes could indicate a systematic error in the test setup. This is further substantiated by the performed scalar calibrations described in section 8 yielding errors below 50nT. Additional tests of full scale range showed this to be above $\pm100000\text{nT}$ – well above the requirement.

7.4 Noise

The noise test is based on the same measurements as the offset test, enabling noise to be measured as a function of temperature as shown in figure 8. Measurement noise remains constant for the main

At temperatures below $-7°\text{C}$, noise level rises to $100 - 150\text{nT}$. This is due to inadequate realignment of the magnetic domains of the sensor, as the set/reset circuit is unable to deliver sufficient current pulses at low temperatures. Because this is only present at relative low temperature and noise remains below 500nT_{peak}, no action has been taken to improve this performance. Any attempt to do so will most likely require higher supply voltage than the 3.6V presently used.

8 Scalar Calibration

Magnetometer calibrations are performed using the method described by Merayo *et al.*[1]. This method is very simple using only a small turn table and the geomagnetic field, and has successfully been used for very high precision magnetometers for magnetic mapping satellites like Ørsted.

The offset vector **O** and rotation/scaling matrix **A** of equation (5) are calculated using numerical methods based on the least square estimator; the resulting orthogonal system is aligned with the intrinsic axes of two of the three sensor axes.

$$\mathbf{B} = \mathbf{A}(\mathbf{EU} - \mathbf{O}) \tag{5}$$

Main requirement for the method to work successfully is evenly distributed measurements, as illustated in figure 9 using magnetometer level calibration points.
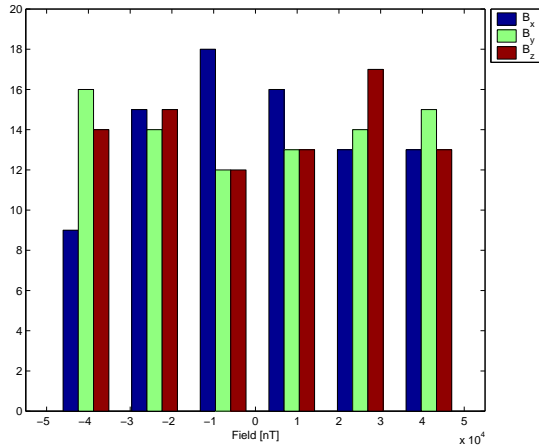
Figure 9: Distribution of measurement points.

8.1 Magnetometer Level Calibration

Magmetometer level calibration is done to verify system performance before satellite integration. Also, this indicates how well the magnetometer performs without disturbances from other subsystems and ferromagnetic objects. Calibration results are given below:

$$\mathbf{O}_{ml} = \begin{bmatrix} 31.71 \\ 199.96 \\ -36.00 \end{bmatrix}$$

$$\mathbf{A}_{ml} = \begin{bmatrix} 4.8327 & -0.0245 & -0.1288 \\ 0 & 4.7857 & -0.1303 \\ 0 & 0 & 4.7689 \end{bmatrix}$$

Non-diagonal elements in **A** can be converted into mis-alignment of the sensors; mis-alignment is below 2° for the magnetometer level calibration.

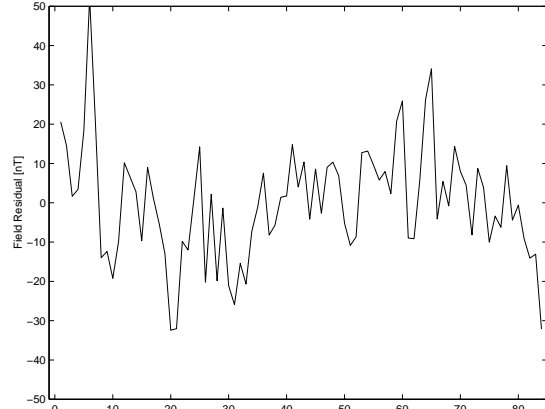The post-calibration residual is shown in figure 10, yielding an accuracy of 50nT.

Figure 10: Residual at magnetometer level.

8.2 Satellite Level Calibration

Final calibration is done using the fully integrated satellite in order to compensate for additional field distortions. Calibration results are given below and show only minor differences compared to the magnetometer calibration:

$$\mathbf{O}_{sl} = \begin{bmatrix} -26.23 \\ 150.89 \\ 74.41 \end{bmatrix}$$

$$\mathbf{A}_{sl} = \begin{bmatrix} 4.8390 & -0.0239 & -0.2222 \\ 0 & 4.8194 & -0.1213 \\ 0 & 0 & 4.7592 \end{bmatrix}$$

Offset has shifted up to 500nT, and mis-alignment has increased to 3° for the satellite level calibration due to ferromagnetic elements. The resulting residual is shown in figure 11, which also yields an absolute accuracy of 50nT.
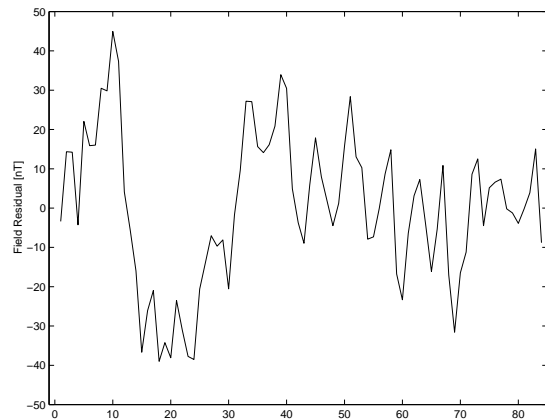

Figure 11: Residual at satellite level.

9 Conclusion

A compact vector magnetometer with accuracy of 50nT, operating ranges of ±100000nT and $-10°$C to 70°C has been constructed for DTUsat. Final satellite level calibration has been performed, and DTUsat is to be launched June 30th, 2003 from Plesetsk, Russia.

The achieved performance is considered to be the current limit of magnetoresistive based magnetometers for small satellites, where size, mass, and power consumption are important factors.

10 Acknowledgements

References

[1] J. M. G. Merayo, P. Brauer, F. Primdahl, J. R. Petersen, and O. V. Nielsen. *Scalar Calibration of Vector Magnetometers*. Technical University of Denmark, Department of Automation., 1999. Published in Meas. Sci. Technol. 11(2000).